Finite mobility effects on the radiative efficiency limit of *pn*-junction solar cells

Julian Mattheis* and Jürgen H. Werner
Institut für Physikalische Elektronik, Universität Stuttgart, 70569 Stuttgart, Germany

Uwe Rau
IEF5-Photovoltaik, Forschungszentrum Jülich, 52425 Jülich, Germany

(Received 2 August 2007; published 8 February 2008)

The maximum power conversion efficiency of a solar cell as defined by the Shockley-Queisser (SQ) radiative recombination limit relies on the assumption that the collection probability for all photogenerated electron/hole pairs is unity. This assumption implies a virtually infinite mobility μ_n of the photogenerated charge carriers. In order to compute the radiative efficiency limit with finite mobilities, we solve the continuity equation for minority carrier transport including an additional photon recycling term that accounts for emission of photons by radiative recombination and their subsequent reabsorption. This approach quantitatively connects the SQ approach with the classical diode theory. Even when assuming radiative recombination as the only loss mechanism, the maximum efficiency achievable within our model is reduced drastically when μ_n drops below a critical value. This critical value depends on the absorption coefficient, the doping density of the absorber material, as well as on the thickness and the light trapping scheme of the solar cell. Thus, these material and device parameters gain a fundamental importance as soon as finite carrier mobility is considered. Our theory yields a criterion that has to be fulfilled by any photovoltaic material in order to guarantee charge separation even in an otherwise most ideal case. Exemplary application of our model to three real photovoltaic materials, crystalline silicon (*c*-Si), amorphous silicon (*a*-Si:H), as well as $Cu(In,Ga)Se_2$ (CIGS), shows that mobilities of *c*-Si and CIGS are three, respectively, 1 order of magnitude above this critical limit whereas the effective hole mobilities in *a*-Si:H are scattered around the critical value. A comparison between solar cells and light-emitting diodes with finite mobility and finite nonradiative lifetime reveals that materials for these complementary devices have to fulfill different requirements.

DOI: 10.1103/PhysRevB.77.085203 PACS number(s): 72.10.Bg, 72.40.+w, 78.60.−b, 84.60.Jt

I. INTRODUCTION

The maximum power conversion efficiency of a solar cell is given by the Shockley-Queisser (SQ) limit.[1] The only quantities defining this theoretical limit are the cell temperature T, the spectral distribution of the solar irradiation, and the band gap energy E_g of the semiconductor acting as the photovoltaic absorber material. The SQ theory is based on the detailed balance between the radiation fluxes absorbed and emitted by the solar cell. The principle of detailed balance states that in thermodynamic equilibrium every process must be in equilibrium with its reverse process. Thus, the SQ limit restricts itself to the absolute minimum of physical actions, namely, the detailed balance pair light absorption and light emission. The elegance of the SQ theory relies on four basic assumptions.

(i) The solar cell absorbs all photons with energy E larger than the band gap energy E_g. Each absorbed photon generates one electron/hole pair.

(ii) Under short circuit conditions all photogenerated carriers contribute to the photocurrent J_{sc}.

(iii) Spontaneous emission of photons by radiative recombination of electron/hole pairs is the only loss mechanism as required by the principle of detailed balance.

(iii) All photons emitted by radiative recombination have the same chemical potential μ. This chemical potential equals the voltage V at the cell's terminals multiplied with the elementary charge q.

At this point it is important to note that all quantities entering into the SQ theory are related to the surface area of the solar cell. The optical and electrical properties hidden underneath this surface are radically idealized by assumptions (i)–(iv). In principle, the solar cell in the SQ sense has a thickness of zero. Therefore, this idealization bears three inherent contradictions.

(a) Since light absorption in any material is described by Beer's law, any light absorption requires a *finite* material thickness. Moreover, an absorptance of strictly unity as required by assumption (i) in principle requires an *infinite* thickness.

(b) Since charge separation cannot occur infinitely fast over a finite distance, a collection probability of unity as required by assumption (ii) can only hold as a limiting case.

(c) Since any carrier transport requires gradients of the electron and hole quasi-Fermi levels E_{Fn} and E_{Fp}, the splitting $\mu=E_{Fn}-E_{Fp}$ cannot exactly correspond to the voltage qV at the cell's terminal as required by assumption (iv).

The SQ limit is often termed as the "radiative recombination limit" for photovoltaic energy conversion. However, the reader may easily recognize that the restriction to radiative recombination is covered by point (iii) from the above list. In turn, assumptions (i), (ii), and (iv) are mere simplifications leading to contradictions (a)–(c). Hence, to circumvent these contradictions and, at the same time, to connect the SQ limit with real solar cells one has to relax assumptions (i), (ii), and (iv). Therefore, a complete approach to the radiative recombination limit of solar cells has to account for the charge carrier transport through the entire thickness of the solar cell. Eventually, such a theory should recover the SQ case as a

 ©2008 The American Physical Society

limiting situation for infinite carrier mobilities and infinite cell thickness.

The present paper investigates the effect of finite mobility μ_n on the conversion efficiency of otherwise ideal solar cells. Whereas the band gap energy E_g is the only material parameter entering the SQ theory, extending the radiative efficiency limit to photovoltaic absorbers with finite μ_n immediately necessitates the inclusion of additional material and device parameters. The thickness of the photovoltaic absorber, the doping density, the applied light trapping scheme, and the absorption coefficient immediately gain fundamental physical importance. The present approach defines a minimum mobility that needs to be surpassed by any given photovoltaic material in order to work optimally as a photovoltaic absorber within a *pn*-junction solar cell. With μ_n being larger than this critical value, the cell efficiencies approach the respective SQ limit if no loss mechanism other than radiative recombination is allowed.

When decreasing the nonradiative lifetime τ_{nr} from infinity to values much smaller than the radiative lifetime τ_r, the model yields a smooth transition from a solar cell that is described by the SQ theory to a solar cell that follows the classical diode theory. The essential ingredient that allows us to make the connection between these two classical theories is the inclusion of photon recycling (PR) into the transport equations as first pointed out by Martí *et al.*[4] We show that neglecting PR within the transport equation as in the classical diode theory is only a good approximation if $\tau_r > 10\tau_{nr}$.

We also use our model to investigate light-emitting diodes (LEDs). In an ideal LED every injected electron is converted into an emitted photon via radiative recombination. Therefore, the ideal solar cell in the SQ sense is at the same time an ideal LED. However, as the presented model points out, the ways in which solar cells and LEDs are affected by finite mobilities and/or finite nonradiative lifetimes differ quite substantially.

This paper is organized as follows. Section II describes the basic ingredients of the present model. A complete account of the rather cumbersome technical details for the model is given in Ref. 22. Section III presents the basic results on the radiative efficiency limit for *pn*-junction solar cells with finite minority carrier mobility μ_n. We demonstrate that the maximum power conversion efficiency of a solar cell is only achievable with μ_n exceeding a certain critical value that in turn depends on the absorption coefficient and the doping density of the photovoltaic absorber material as well as on the thickness and the light trapping scheme of the solar cell. Subsequently, we extend our model to include nonradiative recombination thereby spanning the gap between the SQ theory and the classical textbook description of a *pn*-junction solar cell. We also investigate the consequences of finite mobilities and finite nonradiative lifetimes for solar cells and LEDs. Here we find that upon departure from the ideal situation, solar cells are sensitive to both low lifetimes and low mobilities whereas LEDs are more sensitive to low lifetimes. Section IV shows that our model allows us to investigate the suitability of real materials with finite mobility as photovoltaic absorbers. Here, we use the examples of crystalline silicon (*c*-Si), amorphous silicon (*a*-Si:H), and $Cu(In,Ga)Se_2$ (CIGS). The critical mobilities needed to achieve 90% of the maximum short circuit current in the radiative limit are $\mu_{crit}=0.38\ cm^2\ (V\ s)^{-1}$ for *c*-Si, $\mu_{crit}=0.007\ cm^2\ (V\ s)^{-1}$ for *a*-Si:H, and $\mu_{crit}=0.08\ cm^2\ (V\ s)^{-1}$ for CIGS.

II. DIFFUSION EQUATION WITH REABSORPTION

Most models currently used for the theoretical description of real solar cells are in flat contradiction to the SQ approach. For instance, the most common textbook example for a solar cell[2] uses Shockley's diode theory.[3] The discrepancy between Shockley's diode equation and the SQ theory was addressed by Martí *et al.*[4] The same authors also pointed out that this contradiction is eliminated by the inclusion of PR, i.e., the process of radiative recombination of an electron and/or hole pair followed by the reabsorption of the photon elsewhere in the absorber. Thus, PR introduces a nonlocal radiative interaction term that complements charge carrier transport and establishes the internal and external radiation balance of the photovoltaic absorber.

The effect of PR was discussed theoretically as early as 1957,[5–7] and first experimental evidence was reported ten years later in luminescence measurements.[8–11] The first rigorous theoretical treatment of PR was presented in 1977 by Kuriyama *et al.*[12] who used their theory to analyze luminescence quantum efficiencies in AlGaAs heterostructures. Asbeck[13] derived a (numerical) expression for a modified radiative lifetime that includes reabsorption of photons. Mettler[14] modified the rather complex derivation of Ref. 12 and developed the approach that is also used in the present work.

The relevance of PR for *solar cells* was not investigated until 1991 when Parrott and Potts[15] and Durbin and Gray[16,17] presented simulations of solar cell efficiencies including the effect of PR. These authors restricted themselves to the practical cases where nonradiative recombination is the dominant recombination process. A similar focus was also chosen by Badescu and Landsberg,[18] Yamamoto *et al.*,[19] and Balenzategui and Martí.[20] Parrott[21] was the first to relate photon recycling and the detailed balance efficiency limit. However, while deriving his model for a spatially dependent chemical potential of the emitted photons, all the computations are carried out under the assumptions that the chemical potential of the photons is constant within one absorption length. A constant chemical potential was also assumed in the paper of Martí *et al.*[4] when combining the classical diode theory with detailed balance considerations.

As in this paper, we are also interested in very low values for μ_n; we cannot afford any simplification using only slight spatial variations of the chemical potential of photons. Instead, we use the rigorous approach of Mettler[14] in combination with the numerical computation scheme presented by Durbin and Gray[17] with only minor modifications as pointed out in Ref. 22.

To combine detailed balance considerations and transport of charge carriers, one has to solve the minority carrier diffusion equation

$$D_n \frac{d^2 n}{dx^2} + G_{int}(x) - \frac{n}{\tau_r} - \frac{n - n_0}{\tau_{nr}} = -G_{sun}(x) - G_{bb}(x), \quad (1)$$

complemented by an internal generation rate $G_{int}(x)$ that accounts for the recycling of photons emitted by radiative re-

combination. The detailed derivation of the numerical scheme used to solve this equation with the appropriate boundary conditions is presented in Ref. 22. Here, we restrict ourselves to delineating the basic idea of the approach. For our computations we always neglect the depletion region. This assumption is justified as long as the depletion region is much smaller than the absorption length.

In Eq. (1), $n(x)$ is the profile of the minority carrier concentration over the spatial coordinate x and n_0 is the equilibrium concentration. Transport is exclusively diffusive with the diffusion constant D_n that is related to the electron mobility μ_n via $D_n=(k_BT/q)\mu_n$, where q is the elementary charge, k_B is Boltzmann's constant, and T is the absolute cell temperature. Recombination is split up into radiative recombination with the radiative lifetime τ_r and nonradiative recombination with the nonradiative lifetime τ_{nr}. The external generation consists of the equilibrium blackbody generation rate G_{bb} and the nonequilibrium generation rate G_{sun} provided by the sun. The effect of PR results in an internal generation rate

$$G_{int}(x_g) = \int_{x_r=0}^{x_r=d} \delta G_{int}(x_g,x_r) \tag{2}$$

caused by radiative recombination within the sample. Here, d is the sample thickness and

$$\delta G_{int}(x_g,x_r) = \frac{4\pi\bar{n}^2}{h^3c^2}\int_0^\infty \alpha^2(E)E^2 \exp\left(\frac{-E}{k_BT}\right) \times f_r(x_g,x_r)dE\frac{n(x_r)}{n_0}\delta x_r \tag{3}$$

denotes the generation rate at $x=x_g$ that is caused by radiatively recombining carriers in x_r. Here, $\bar{n}$ is the refractive index, h is Planck's constant, c is the speed of light, E is the photon energy, and $\alpha(E)$ is the absorption coefficient. The interaction term embraces all interaction paths between the coordinates x_r and x_g. The computation of these interaction terms is somewhat cumbersome. For the plane surface [Fig. 1(a)] we refer to the work of Durbin and Gray.[17] For the case of a textured surface [Fig. 1(b)], we restrict ourselves to give the results of our analysis that can be found elsewhere.[22]

In the following, we denote the two light paths that connect x_r and x_g with no intermediate reflection at the front surface as "direct" [cf. Figs. 1(a) and 1(b)]. Under the assumption of a perfectly reflecting back side, integrating this interaction term across all spherical angles yields

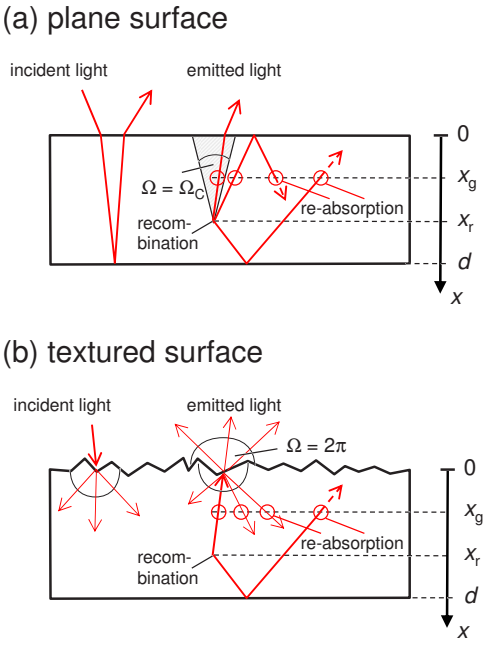

FIG. 1. (Color online) In a solar cell with plane surface (a) all external rays impinging on the front surface are refracted toward the surface normal due to the higher refractive index $\bar{n}$ inside the semiconductor. Internally emitted rays leave the cell if the emission angle is smaller than the critical solid angle $\Omega_c=2\pi\arcsin(1/\bar{n})$. If the emission angle is larger than Ω_c then the ray is internally reflected until it is completely absorbed within the solar cell. In a cell with textured surface (b) an external ray is randomized upon transmitting the front surface. The same accounts for internally emitted rays. These internal rays are transmitted with the transmission probability t_{Lamb} into the half sphere with $\Omega=2\pi$ and reflected with the probability $1-t_{Lamb}$.

$$f_r^{dir}(x_g,x_r,E) = \mathrm{Ei}(\alpha(E)|x_g-x_r|) + \mathrm{Ei}(\alpha(E)(2d-x_g-x_r)), \tag{4}$$

where

$$\mathrm{Ei}(z) = \int_z^\infty \frac{\exp(-t)}{t}dt \tag{5}$$

denotes the exponential integral.

All paths that involve reflections at the front surface depend on the assumed optical properties of that surface. The indirect interaction terms of a flat surface [Fig. 1(a)] are given in Ref. 17. For the Lambertian light trapping [Fig. 1(b)], we find (see Appendix and Refs. 22 and 23)

$$f_r^{Lamb}(x_g,x_r,E) = \frac{2\{\mathrm{Ei}_2(\alpha x_r)+\mathrm{Ei}_2(2\alpha d-\alpha x_r)\}\{\mathrm{Ei}_2(\alpha x_g)+\mathrm{Ei}_2(2\alpha d-\alpha x_g)\}}{1-t_{cell}(1-t_{Lamb})}, \tag{6}$$

where the function $\mathrm{Ei}_2(z)$ is defined by $\mathrm{Ei}_2(z)=\exp(-z)-z\,\mathrm{Ei}(z)$. The average transmission probability t_{Lamb} of a Lambertian surface with zero reflectance is $t_{Lamb}=1/\bar{n}^2$. The transmission probability t_{cell} through the cell averaged over a Lambertian angular distribution of the light is

TABLE I. Standard parameters used for the computations. The parameters include the band gap E_g, the refractive index $\bar{n}$, the cell thickness d, the reflection coefficients ϱ_f at the front surface and ϱ_b at the back side, and the electron surface recombination velocity S_n at the back contact.

E_g	$\bar{n}$	d	ϱ_f	ϱ_b	S_n	$\alpha(E)$	Front surface
1 eV	3	$10/\alpha_0$	0	1	0	α_0	Textured

$$t_{cell} = (1 - 2\alpha d)\exp(-2\alpha d) + (2\alpha d)^2\,\mathrm{Ei}(2\alpha d). \quad (7)$$

The generation rates G_{sun} and G_{bb} on the right hand side of Eq. (1) are computed in a similar manner as the internal generation rate G_{int} and include multiple reflections as well.[22]

To solve the linear integrodifferential equation [Eq. (1)], we transform it into a self-consistent matrix equation that includes the optical interaction between the planes at x_r and x_g with finite thickness Δx. The numerical evaluation scheme is closely related to the procedure used by Durbin and Gray.[16,17]

III. RESULTS WITH CONSTANT ABSORPTION COEFFICIENT

A. Basic assumptions

This section discusses the results of the computations. For the analysis we normalize the mobility μ_n to the reference mobility[22]

$$\mu_{ref} = \frac{qN_A\Phi_{bb}^{E_g}}{k_B T\alpha_0 n_i^2}, \quad (8)$$

where N_A is the doping concentration, n_i is the intrinsic carrier concentration, $\Phi_{bb}^{E_g}$ is the integrated blackbody spectrum $\Phi_{bb}^{E_g} = \int_{E_g}^{\infty}\phi_{bb}(E)dE$ with $\phi_{bb}(E)$ being the spectral blackbody photon density, and α_0 is the absorption coefficient at a photon energy $E = E_g + k_B T$. In this section, we restrict the discussion to the case of constant absorption coefficient $\alpha(E) = \alpha_0$ for $E \geqslant E_g$ and $\alpha(E) = 0$ for $E < E_g$. For constant absorption, the reference mobility is expressed in terms of the radiative lifetime τ_r and reads as

$$\mu_{ref} = \frac{qN_A}{4k_B T\bar{n}^2\alpha_0^2 n_i^2\tau_r}. \quad (9)$$

We begin the analysis with the radiative efficiency limit, i.e., with radiative recombination being the only loss mechanism. For a sufficiently thick sample that guarantees virtually complete light absorption, we investigate the influence of mobility and band gap energy. Subsequently, we analyze the impact of reduced sample thickness, combined with light trapping effects of a randomly textured front surface. Finally, we discuss the influence of nonradiative recombination.

If not mentioned otherwise, all simulations use the parameters listed in Table I. All simulations assume a *pn*-junction solar cell with *p*-type base, no recombination in the space charge region or at the back contact, and no parasitic Ohmic losses. We further assume perfect optical surfaces, i.e., a reflection coefficient $\varrho_f = 0$ at the front surface and $\varrho_b = 1$ at the back surface.

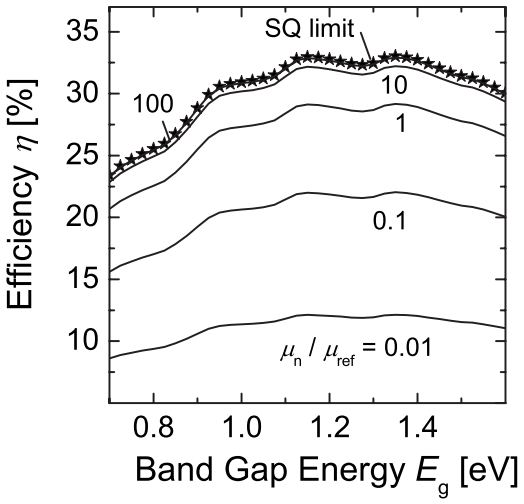

FIG. 2. Radiative efficiency (no nonradiative recombination) vs band gap energy E_g. The absorption coefficient is $\alpha = \alpha_0$, the normalized thickness is $\alpha_0 d = 10$, and the front surface is textured. All parameters are listed in Table I. For increasing mobility, the efficiency approaches the Shockley-Queisser limit (stars). For lower normalized mobilities, however, the efficiency is reduced drastically, even though radiative recombination is the only loss mechanism. The efficiency loss is caused by reduced carrier collection manifested in a reduced short circuit current J_{sc}.

B. Radiative efficiency limit

Figure 2 displays the SQ efficiency limit for an AM1.5G spectrum[24] versus the band gap energy (stars). Also shown are the simulation results for a solar cell with radiative recombination as the only loss mechanism [assumption (iii)] but with finite mobility μ_n. For $\mu_n > 100\mu_{ref}$ the efficiency equals the efficiency limit calculated by Shockley and Queisser. The large thickness $\alpha_0 d = 10$ guarantees complete light absorption [assumption (i)] and the large mobility guarantees complete collection of the generated carriers [assumptions (ii) and (iv)]. The inclusion of photon recycling guarantees the fulfillment of the detailed internal and external radiation balance. Thus, all assumptions of the SQ theory are fulfilled. Upon decreasing the mobility μ_n, carrier collection is diminished, which leads to a reduction in the short circuit current density J_{sc} and consequently to a reduction in the efficiency.

Figure 3 demonstrates the influence of the mobility on the short circuit and the saturation current density J_0 that determines the recombination current via the diode law

$$J = J_0\exp[qV/(k_B T)] - 1. \quad (10)$$

The figure shows J_0 and J_{sc} normalized to their maximum values J_0^{SQ} and J_{sc}^{SQ} in the SQ limit versus the mobility μ_n/μ_{ref}. For sufficiently large mobilities the normalized currents approach unity, i.e., the Shockley-Queisser limit. However, reducing the mobility below a critical value

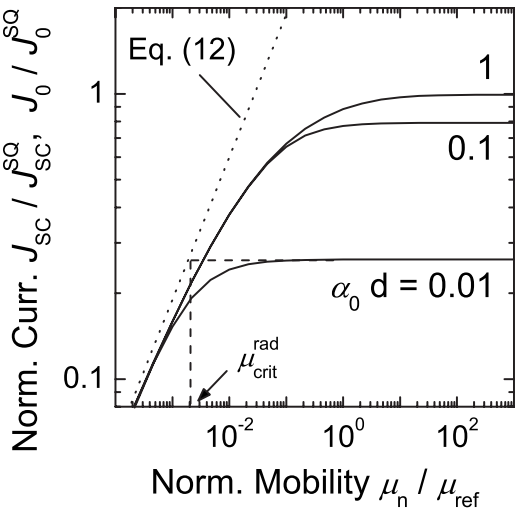

FIG. 3. Short circuit current J_{sc} and saturation current J_0 normalized to the maximum currents in the Shockley-Queisser limit vs the normalized mobility μ_n/μ_{ref}. The currents approach their maximum value for sufficiently large mobility. With decreasing mobility, both short circuit current and saturation current drop sharply once μ_n falls below a critical mobility μ_{crit}^{rad}. The absorption coefficient is $\alpha=\alpha_0$, the band gap is $E_g=1$ eV, and the front surface is textured. All parameters are taken from Table I.

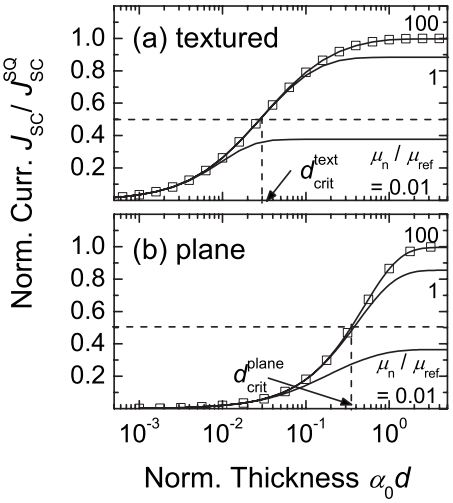

FIG. 4. Currents J_0 and J_{sc} normalized to the maximum values in the Shockley-Queisser limit vs cell thickness d for a textured (a) and plane (b) front surface. The absorption coefficient is $\alpha=\alpha_0$ and the band gap is $E_g=1$ eV; all other parameters are listed in Table I. For low d, the currents are limited by the incomplete absorptance of the cell (squares). For low mobilities, the current saturates at lower levels. This is because once the sample thickness is larger than the diffusion length, further increase of the thickness will not lead to increased carrier collection even though the absorption might still be increased.

$$\mu_{crit}^{rad} = \frac{\mu_{ref}}{4\bar{n}^2}a^2(d) = \frac{q\Phi_{bb}^{E_g}N_A}{4\bar{n}^2k_BT\alpha_0 n_i^2}a^2(d) \tag{11}$$

results in a sharp drop of the extracted currents. The value of the critical mobility depends on the absorptance $a(d)$ [cf. Eqs. (13) and (15)] and is obtained from the intersect of the low-mobility limit[22]

$$J_0^{rad}/J_0^{SQ} = 2\bar{n}\sqrt{\mu_n/\mu_{ref}}, \tag{12}$$

with the high-mobility limit $J_0^{rad}/J_0^{SQ}=a(d)$ as exemplarily depicted in Fig. 3 for $\alpha_0 d=0.01$. At $\mu_n=\mu_{crit}^{rad}$ it holds $J_{sc}=0.5a(d)J_{sc}^{SQ}$ and $J_0^{rad}=0.5a(d)J_0^{SQ}$.

Due to the assumed spectral independence of the absorption coefficient $\alpha(E)=\alpha_0$ and the textured front surface, the generation profiles caused by ambient room temperature blackbody and solar irradiation are identical except for their magnitude. Therefore, J_0 and J_{sc} exhibit the same dependency on μ_n/μ_{ref} and, thus, the open circuit voltage $V_{oc}=(k_BT/q)\ln(J_{sc}/J_0+1)$ is independent of the mobility. Consequently, the reduction of the efficiency with decreasing μ_n is exclusively caused by the reduction of the short circuit current.

C. Light trapping

The enhanced light trapping by textured surfaces normally serves to reduce the cell thickness that is necessary to absorb a sufficiently large part of the available sunlight. Therefore, Figs. 4(a) and 4(b) investigate the effect of light trapping by comparing the dependence of the short circuit current density J_{sc} on the normalized cell thickness $\alpha_0 d$ of a textured and a nontextured cell. For high mobilities $\mu_n=100\mu_{ref}$, J_{sc} of both cells follows the absorptance [shown as open squares in Figs. 4(a) and 4(b)].

The absorptance $a(d)$ depends on the thickness d and the nature of the front surface. For a textured front surface with $\varrho_f=0$ and a back side with $\varrho_b=1$ it holds[22,25]

$$a(d) \approx \frac{d}{d+d_{crit}^{text}}, \tag{13}$$

where the critical thickness

$$d_{crit}^{text} = \frac{1}{4\alpha_0\bar{n}^2} \tag{14}$$

is defined as the thickness at which it holds $a(d)=0.5$.

For normal incidence on a plane front surface with $\varrho_f=0$ and $\varrho_b=1$, the absorptance reads as

$$a(d) = 1 - \exp(-2\alpha_0 d). \tag{15}$$

From $a(d_{crit}^{plane})=0.5$ we obtain from Eq. (15) the critical thickness

$$d_{crit}^{plane} = \frac{\ln(2)}{2\alpha_0}. \tag{16}$$

As can be seen from Fig. 4, the critical thickness d_{crit}^{text} for the textured front surface is by roughly a factor of 10 smaller than d_{crit}^{plane} for the nontextured surface. This effect is due to two reasons. First, the incident light is diffracted and traverses the sample at an angle, thus experiencing a longer propagation path than light with normal incidence on a plane surface. Second, all rays are internally reflected at the front

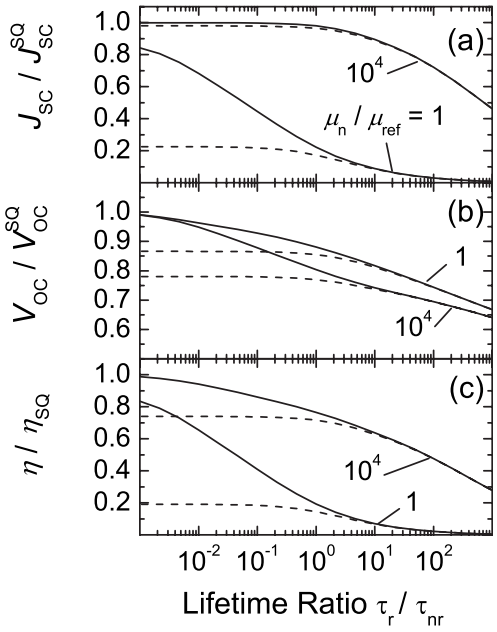

FIG. 5. Solar cell output parameters vs the lifetime ratio of radiative and nonradiative lifetimes for different normalized mobilities $\mu_{norm}=1$ and $\mu_{norm}=10^4$. Solid lines represent the numerical calculations including photon recycling (PR), and dashed lines stand for the classical approach (Ref. 3) obtained by leaving out the PR term. The classical approach yields reasonable results only if the radiative lifetime is at least ten times larger than the nonradiative lifetime, i.e., for $\tau_r > 10\tau_{nr}$. Whereas losses in the short circuit current J_{sc} for low lifetimes can be compensated by increasing the mobility (a), the open circuit voltage is almost exclusively dominated by the lifetime (b). For high mobilities, the efficiency is limited by V_{oc}, for low mobilities, J_{sc} is the limiting factor (c). The absorption coefficient is $\alpha=\alpha_0$, the normalized thickness is $\alpha_0 d=10$, the band gap is $E_g=1$ eV, and the front surface is textured. All parameters are listed in Table I.

surface with the increased reflection coefficient $1-1/\bar{n}^2$,[26] leading to efficient light trapping within the sample. From Eqs. (14) and (16) we find $d_{crit}^{plane}/d_{crit}^{text}=2\ln(2)\bar{n}^2\approx 12.5$ with the refractive index $\bar{n}=3$.

We also observe in Fig. 4 that the achievable J_{sc} values for the smaller mobilities $\mu_n=1(0.01)\times\mu_{ref}$ are slightly higher for the textured compared to the nontextured cell. Thus, textured solar cells display a larger tolerance to low mobilities than nontextured cells. However, the major benefit of light trapping is the allowance for thinner cells in the nonradiative[26] as well as in the radiative limit.

D. Nonradiative recombination

Figures 5(a)–5(c) illustrate how the efficiency η, the short circuit current density J_{sc}, and the open circuit voltage V_{oc} depend on the ratio of radiative and nonradiative lifetimes (solid lines). The quantities are displayed for the two normalized mobilities $\mu_n/\mu_{ref}=1$ and $\mu_n/\mu_{ref}=10^4$. With increasing nonradiative recombination the short circuit current in Fig. 5(a) decreases due to the decreasing diffusion length and the resulting reduced carrier collection. However, for J_{sc}, only the diffusion length, i.e., the product of mobility and lifetime, is relevant, and, thus, the losses induced by decreasing lifetime are compensated with high mobility. Therewith, almost complete carrier collection is achieved even with miserable lifetimes. The critical mobility needed to maintain sufficient carrier collection depends on the nonradiative lifetime and for thick solar cells with $a(d)=1$ reads as[22]

$$\mu_{crit}=\mu_{crit}^{rad}+\frac{\mu_{ref}\bar{n}^2\tau_r}{\tau_{nr}}. \tag{17}$$

The critical mobility approaches its radiative limit μ_{crit}^{rad} for $\tau_{nr}\gg\tau_r$. With increasing nonradiative recombination, i.e., $\tau_{nr}\ll\tau_r$, μ_{crit} is proportional to τ_r/τ_{nr} and is expressed as a critical diffusion length

$$L_{crit}=\sqrt{\frac{k_BT\mu_{crit}\tau_{nr}}{q}}=\sqrt{\frac{k_BT\mu_{ref}\bar{n}^2\tau_r}{q}}=\frac{1}{\alpha_0}, \tag{18}$$

which equals the absorption length $1/\alpha_0$.

The open circuit voltage V_{oc} decreases with increasing nonradiative recombination as well [Fig. 5(b)]. While the mobility has no influence on V_{oc} in the radiative limit, the open circuit voltage is slightly higher for lower mobilities when nonradiative recombination comes into play. However, the mobility by no means has the compensating effect it has on the short circuit current. For the open circuit voltage the crucial factor is definitely the lifetime. Since both J_{sc} and V_{oc} decrease with increasing nonradiative recombination, also the efficiency is decreased [Fig. 5(c)]. For high mobilities, η is dominated by V_{oc} as long as the short circuit current remains high ($\mu_n>\mu_{crit}$). For low mobilities, however, the efficiency is dominated by the drastic losses in J_{sc}.

For comparison, the results from the classical diode theory[3] are displayed as well (dashed lines). In this context, classical diode theory means leaving out the internal generation rate G_{int} in Eq. (1) that is caused by photon recycling. If recombination is dominated by nonradiative recombination, i.e., for $\tau_r>10\tau_{nr}$, photon recycling is negligible and the classical diode theory is sufficiently accurate; the results with or without the inclusion of photon recycling converge. With decreasing nonradiative recombination, radiative recombination and PR become much more important. The classical diode theory is not sufficient to describe the efficiency in the radiative limit. In the form chosen here, the classical theory predicts efficiencies that are far below the SQ limit.

E. Reciprocity between solar cell and light-emitting diode

Although solar cells and LEDs are reciprocal devices converting optical energy into electrical energy and vice versa, this does not automatically imply that both devices have the same material requirements in terms of lifetime and mobility. This section analyzes the relationship between solar cell and LED performance and points out the different material criteria to obtain high performance devices.

Whereas the performance of a solar cell is measured by its power conversion efficiency η, the performance of a light-emitting diode is not quantified in energy terms but in terms of the (external) LED quantum efficiency

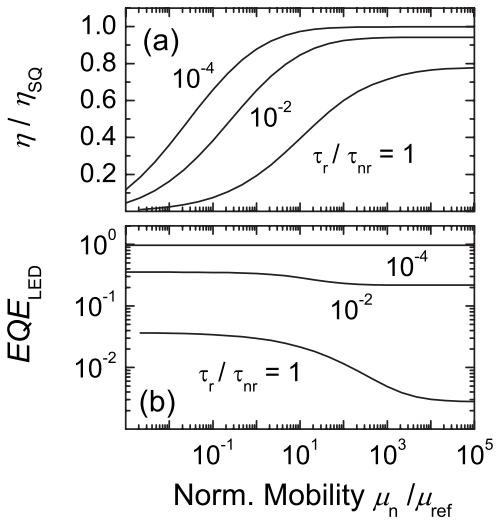

FIG. 6. Solar cell efficiency η/η_{SQ} (a) and LED quantum efficiency EQE_{LED} (b) versus the normalized mobility μ_n/μ_{ref}. The power conversion efficiency η decreases with decreasing mobility. This decrease is more pronounced at low lifetimes. In contrast, the quantum efficiency EQE_{LED} depends almost exclusively on the nonradiative carrier lifetime. The absorption coefficient is $\alpha=\alpha_0$, the normalized thickness is $\alpha_0 d=10$, the band gap is $E_g=1$ eV, and the front surface is textured. All parameters are identical to the parameters used in Fig. 5.

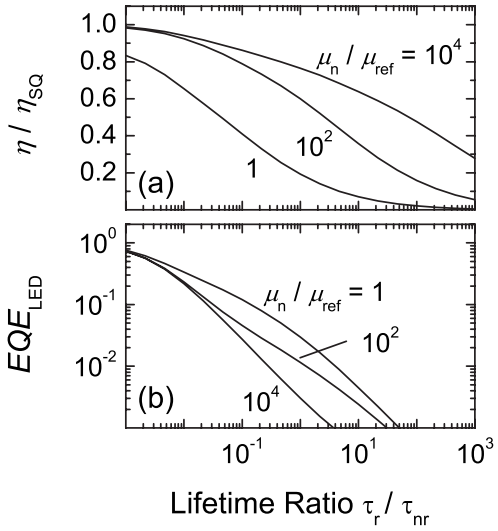

FIG. 7. Solar cell efficiency η/η_{SQ} (a) and LED quantum efficiency EQE_{LED} (b) versus the lifetime ratio of radiative and nonradiative lifetimes. Whereas the decrease of the power conversion efficiency η caused by nonradiative recombination can be compensated by a sufficiently high mobility μ_n, the quantum efficiency EQE_{LED} depends almost exclusively on the nonradiative carrier lifetime and is hardly influenced by the mobility. All parameters are identical to the parameters used in Fig. 6.

$$EQE_{LED} = \frac{\Phi_{em}(V) - \Phi_{bb}^{E_g}}{J_{el}(V)/q}, \tag{19}$$

which states which part of the electrical current density J_{el} at the terminals of the device is converted into the excess emission flux density $\Phi_{em}-\Phi_{bb}^{E_g}$. As shown in Refs. 27 and 28 the LED quantum efficiency is coupled to the open circuit voltage of a solar cell via

$$EQE_{LED} = \frac{J_0^{rad}}{J_0^{rad} + J_0^{nr}} \approx \exp\left[\frac{q}{k_B T}(V_{oc} - V_{oc}^{rad})\right], \tag{20}$$

where V_{oc}^{rad} is the open circuit voltage that would be achieved if the device were dominated by radiative recombination only. In a first order approximation, V_{oc}^{rad} is equal to V_{oc}^{SQ}.[27,28] Relation (20) demonstrates that the LED quantum efficiency EQE_{LED}, i.e., the quality of an LED, is coupled directly to the open circuit voltage of the device when acting as a solar cell. Therefore, the crucial material parameter to obtain a good quantum efficiency EQE_{LED} is—just as for the open circuit voltage V_{oc}—the lifetime ratio τ_r/τ_{nr}. This result is insofar as not surprising as the lifetime ratio also determines the internal LED quantum efficiency $IQE_{LED}=(1+\tau_r/\tau_{nr})^{-1}$, which describes the probability that a recombination event takes place radiatively.

Figures 6(a) and 6(b) display the normalized solar cell efficiency η/η_{SQ} (a) and the LED quantum efficiency EQE_{LED} (b) vs the normalized mobility μ_n/μ_{ref}. Figure 6(a) demonstrates a significant deterioration of the photovoltaic efficiency η when decreasing the mobility μ_n. This effect results from the decline of the short circuit current density J_{sc} that enters linearly into the output power, and hence into the efficiency of the solar cell. The effect of μ_n on η depends also on the lifetime ratio τ_r/τ_{nr}. However, even for $\tau_r/\tau_{nr}=10^{-4}$, i.e., basically in the radiative limit, η drops sharply as soon as μ_n/μ_{ref} becomes smaller than unity. Interestingly, the LED quantum efficiency EQE_{LED} at this lifetime ratio is basically unaffected by any mobility effect as can be seen in Fig. 6(b). Only for $\tau_r/\tau_{nr}=10^{-2}$ and 10^0 we notice an influence of μ_n on EQE_{LED}. This mobility effect, however, is much less pronounced than the consequences of the variations of the ratio τ_r/τ_{nr} that cause the differences between the different curves in Fig. 6(b). In addition, lowering the mobility implies an *increase* of EQE_{LED} which is in sharp contrast to the mobility effect on η in Fig. 6(a).

The influence of the lifetime ratio τ_r/τ_{nr} on η and EQE_{LED} is illustrated in Figs. 7(a) and 7(b). Obviously, both quantities deteriorate with increasing τ_r/τ_{nr}, i.e., with increasing contribution of nonradiative recombination. However, the sensitivity of the solar cell efficiency η on the increase of nonradiative recombination is much less pronounced than that of the LED quantum efficiency EQE_{LED}. This is because, especially for high mobilities [$\mu_n/\mu_{ref}=10^4$ and 10^2 in Fig. 7(a)] the product $\mu_n\tau$ that defines the diffusion length is still large enough to warrant almost complete carrier collection. Thus, even down to a relatively low lifetime the short circuit current is barely affected by decreasing τ_{nr} [cf. Fig. 5(a)]. In contrast, the open circuit voltage V_{oc} is affected by a decrease of τ_{nr} already at very large values of τ_{nr} [cf. Fig. 5(b)]. It is interesting to discuss the curves in Fig. 7(b) with respect to their reciprocal interpretation for the LED quantum efficiency EQE_{LED} and for the photovoltaic open circuit voltage V_{oc} as depicted in Fig. 5(b). Obviously, an increase of non-

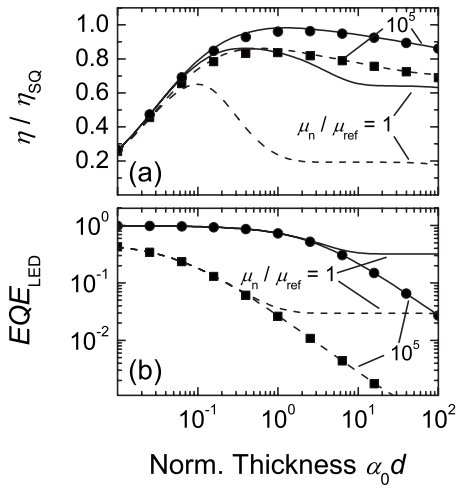

FIG. 8. Solar cell efficiency η/η_{SQ} (a) and LED quantum efficiency EQE_{LED} (b) versus the normalized thickness $\alpha_0 d$ for different lifetime ratios $\tau_r/\tau_{nr}=10^{-2}$ (solid lines) and $\tau_r/\tau_{nr}=1$ (dashed lines). A second parameter is the normalized mobility $\mu_n/\mu_{ref}=1$ and $\mu_n/\mu_{ref}=10^5$ as indicated in the figure. For decreasing absorber thickness, the efficiency (a) is limited by incomplete absorption. In contrast, the LED quantum efficiency (b) converges toward the internal quantum efficiency given by $IQE_{LED}=(1+\tau_r/\tau_{nr})^{-1}$. With increasing sample thickness, nonradiative bulk recombination leads to a decrease in both η and EQE_{LED}. Symbols represent the analytical approximations in the high-mobility limit. The absorption coefficient is $\alpha=\alpha_0$, the band gap is $E_g=1$ eV, and the front surface is textured.

radiative recombination (increasing ratio τ_r/τ_{nr}) leads to a dramatic decline of EQE_{LED}. The interpretation of the same data in terms of V_{oc} is pronouncedly less dramatic. We have only a loss of about 60 mV in V_{oc} where we loose a factor of 10 in EQE_{LED}. This is because of the exponential relation between V_{oc} and EQE_{LED} as given by Eq. (20).

Thus, we may summarize Figs. 6 and 7 as follows: When departing from the ideal limit ($\mu_n=\infty$, $\tau_{nr}=\infty$, where $EQE_{LED}=1$ and $\eta=\eta_{SQ}$), LEDs are especially sensitive to decreasing τ_{nr}, whereas they are rather insensitive to a decrease of μ_n. On the contrary, a decrease of μ_n leads to considerable losses in the photovoltaic conversion efficiency η of solar cells. Moreover, solar cells are less prone to an increase of nonradiative recombination.

F. Thickness of solar cells and light-emitting diodes

As Fig. 7(b) demonstrates, the external LED quantum efficiency already drops drastically at $\tau_r/\tau_{nr}=10^{-2}$, even though the corresponding internal quantum efficiency $IQE_{LED}=0.99$ is close to unity. This effect stems from the fact that only a fraction of the internally emitted photons directly leave the device if the thickness exceeds $1/\alpha_0$. Reabsorption of those photons then multiplies the consequences of nonradiative recombination.

Figures 8(a) and 8(b) demonstrate the influence of the absorber thickness on solar cell efficiency (a) and on LED quantum efficiency (b). Both η and EQE_{LED} are displayed for the lifetime ratios $\tau_r/\tau_{nr}=10^{-2}$ (solid lines) and $\tau_r/\tau_{nr}=1$ (dashed lines), and for the normalized mobilities $\mu_n/\mu_{ref}=1$ and $\mu_n/\mu_{ref}=10^5$.

For decreasing sample thickness, the efficiency in Fig. 8(a) is limited by incomplete absorption. Neither mobility nor lifetime have an influence on η. With increasing thickness, the absorptance increases which in turn results in a higher short circuit current and efficiency. For low lifetimes, further increase of the thickness results in increased nonradiative bulk recombination which reduces the open circuit voltage and consequently, the efficiency until the thickness surpasses the diffusion length. The combined effect of the mobility on V_{oc} and on J_{sc} in total leads to a positive influence of the mobility on the efficiency and to a lowered reduction of η with d for high mobilities.

In contrast, in Fig. 8(b) the external quantum efficiency EQE_{LED} approaches its maximum value, the internal quantum efficiency IQE_{LED}, for $\alpha_0 d \to 0$. This is because PR effects become negligible for $\alpha_0 d \to 0$ and all internally emitted photons are also emitted externally. It holds $IQE_{LED}=0.99$ for $\tau_r/\tau_{nr}=10^{-2}$ and $IQE_{LED}=0.5$ for $\tau_r/\tau_{nr}=1$. Again, with increasing thickness, nonradiative bulk recombination reduces EQE_{LED} until the thickness surpasses the diffusion length. Hence, low mobilities, leading to lower diffusion lengths, mitigate this effect in LEDs.

Let us perform an analytical approximation to point out the dependency of the solar cell efficiency and the LED quantum efficiency on thickness and lifetime for the case of $\mu_n \to \infty$. With this simplification, the radiative saturation current density for an energy-independent absorption coefficient $\alpha(E)=\alpha_0$ for $E>E_g$ (Refs. 1 and 25) is given by

$$J_0^{rad} = J_0^{SQ} = \frac{2\pi q k_B T a(d)}{h^3 c^2} \exp\left(\frac{-E_g}{k_B T}\right)[E_g^2 + 2E_g k_B T + 2(k_B T)^2]. \tag{21}$$

Using the radiative lifetime[29]

$$\tau_r = \left\{ \frac{8\pi k_B T \bar{n}^2 \alpha_0}{h^3 c^2} \exp\left(\frac{-E_g}{k_B T}\right)[E_g^2 + 2E_g k_B T + 2(k_B T)^2] \right\}^{-1} \tag{22}$$

and the absorptance $a(d)$ of a textured sample from Eq. (13), we obtain

$$J_0^{rad} = \frac{q n_0 a(d)}{4\bar{n}^2 \alpha_0 \tau_r} = \frac{q n_0 d}{(1+4\bar{n}^2 \alpha_0 d)\tau_r}. \tag{23}$$

The nonradiative saturation current for $\mu_n \to \infty$ is simply given by

$$J_0^{nr} = \frac{q n_0 d}{\tau_{nr}}. \tag{24}$$

In the high-mobility limit, the power conversion efficiency is obtained with help of $J_{sc}=a(d)J_{sc}^{SQ}$ and $V_{oc}=(k_B T/q)\ln[J_{sc}/(J_0^{rad}+J_0^{nr})]$. Figure 8(a) demonstrates the good agreement between analytical (symbols) and numerical (lines) results.

Accordingly, the LED quantum efficiency reads as

$$\mathrm{EQE}_{\mathrm{LED}} = \frac{1}{1 + J_0^{\mathrm{nr}}/J_0^{\mathrm{rad}}} = \frac{1}{1 + (1 + 4\bar{n}^2\alpha_0 d)\,\tau_r/\tau_{\mathrm{nr}}}. \quad (25)$$

Figure 8(b) displays $\mathrm{EQE}_{\mathrm{LED}}$ computed with Eq. (25) as symbols. For $\mu_n/\mu_{\mathrm{ref}}=10^5$, the analytical solution shows an excellent agreement with the numerical values. For $\mu_n/\mu_{\mathrm{ref}}=1$, the results differ once the thickness exceeds the diffusion length.

The considerations of this and the preceding section show that the material and device requirements to obtain a good light-emitting diode are not necessarily equivalent to the requirements necessary to obtain a good solar cell. An LED primarily requires a high lifetime. It profits from increased $\mathrm{EQE}_{\mathrm{LED}}$ with reduced thickness and might even gain from a lower carrier mobility. In contrast, a solar cell should be thick enough to guarantee almost complete light absorption. Also, a high lifetime alone is not sufficient to make a good solar cell. The solar cell additionally needs a high carrier mobility. In a solar cell it is not enough to prevent nonradiative recombination. One also has to ensure the transport of photogenerated minority carriers out of the cell. Moreover, a solar cell should be considerably thicker than an LED, in particular, for high mobilities.

IV. MAXIMUM EFFICIENCIES OF REAL MATERIALS

This section analyzes the critical mobility and the efficiency limits for the three semiconducting materials crystalline silicon (*c*-Si), hydrogenated amorphous silicon (*a*-Si:H), and $\mathrm{Cu}(\mathrm{In}_{1-x},\mathrm{Ga}_x)\mathrm{Se}_2$ with $x=0.26$ (CIGS). It investigates whether any of the three materials is limited by the minority carrier mobility in the radiative recombination limit or whether insufficient carrier transport is only a problem in combination with low carrier lifetimes. These considerations are particularly important with respect to the efficiency potential of *a*-Si:H and CIGS, two materials with relatively low reported mobility values.

The cell thicknesses are chosen as typical values and also large enough to guarantee virtually complete absorption of the solar spectrum. We use $d=200$ μm for *c*-Si, $d=1$ μm for *a*-Si:H, and $d=2$ μm for CIGS. All solar cells are assumed to be *pn*-junction solar cells with a zero reflectance textured front surface, and no recombination at the back contact. The absorption coefficients are taken from Ref. 2 in the case of crystalline silicon or from measured data and are displayed in Fig. 9. The measured data include sub-band-gap tail-like absorption. For the simulation we assume that all carriers excited into these states contribute to the photo current with the same mobility as those excited into states in the conduction or valence band. Other parameters needed for the simulation are taken from Ref. 30 in the case of *c*-Si, from Refs. 31 and 32 in the case of *a*-Si:H, and from Ref. 33 in the case of CIGS. A detailed listing of the parameters is given in Ref. 22.

For the transformation of the normalized mobility μ_n/μ_{ref} and the lifetime ratio $\tau_r/\tau_{\mathrm{nr}}$ into the unit-bearing quantities μ_n, τ_r, and τ_{nr}, one requires the doping concentration N_A. We assume $N_A=5\times10^{16}$ cm^{-3} which is a typical value for silicon solar cells. However, the doping concentration must not be chosen too low in order not to violate the assumption of low-level injection, in particular, in the radiative recombination limit. For a given doping concentration, the exact dependence on μ_n and τ_{nr} is only captured below a maximum open circuit voltage $V_{\mathrm{oc}}^{\mathrm{max}}=(2k_BT/q)\ln(N_A/n_i)$. A generalized approach that is not limited to low-level injection will be presented in Ref. 34.

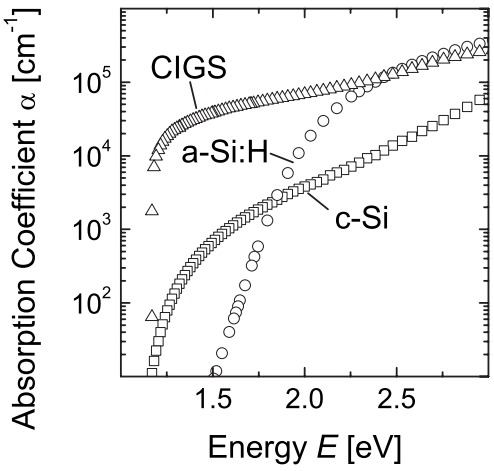

FIG. 9. Experimental absorption coefficients of crystalline silicon (*c*-Si, squares), hydrogenated amorphous silicon (*a*-Si:H, circles), and $\mathrm{Cu}(\mathrm{In}_{1-x},\mathrm{Ga}_x)\mathrm{Se}_2$ (CIGS, triangles) with $x=0.26$ versus the photon energy. Amorphous silicon exhibits a significant sub-band-gap absorption in band tail states. In the chosen spectrum of CIGS the band tails are much less pronounced.

Figures 10(a)–10(c) display the simulated efficiency η versus the nonradiative lifetime τ_{nr} for different mobilities. The chosen mobilities vary between the materials and are chosen in such a way that reported measured values fall in the displayed range. The mobilities are $\mu_n=24$, 240, and 2400 cm^2 (V s)$^{-1}$ for *c*-Si, $\mu_n=0.34$, 3.4, and 34 cm^2 (V s)$^{-1}$ for *a*-Si:H, and $\mu_n=0.15$, 1.5, and 150 cm^2 (V s)$^{-1}$ for CIGS. The unconventional values result from the denormalization of the normalized mobilities.

Figures 11(a)–11(c) depict the critical mobilities extracted from the simulations as a function of the nonradiative lifetime τ_{nr}. Open symbols represent the mobility at which the short circuit current has reached 90% of its maximum value and solid symbols represent the mobility at which the current has reached 50%. Note that Eqs. (9) and (17) are not strictly valid for energy-dependent absorption coefficient and only convey the general picture of the involved dependencies.

A. Crystalline silicon

Monocrystalline silicon has a very high electron mobility $\mu_n=1240$ cm^2 (V s)$^{-1}$.[30] With passivated surfaces, at a doping density $N_A=5\times10^{16}$ cm^{-3}, lifetimes of several hundreds of microseconds are attainable (see, for example, Ref. 35). Therefore, collection of almost all photogenerated charge carriers is usually warranted in *c*-Si solar cells. In Fig. 11(a), the critical mobility $\mu_{\mathrm{crit}}(90\%)$, which allows us to extract 90% of those carriers, for $\tau_{\mathrm{nr}}\to\infty$ saturates at $\mu_{\mathrm{crit}}^{\mathrm{rad}}(90\%)$

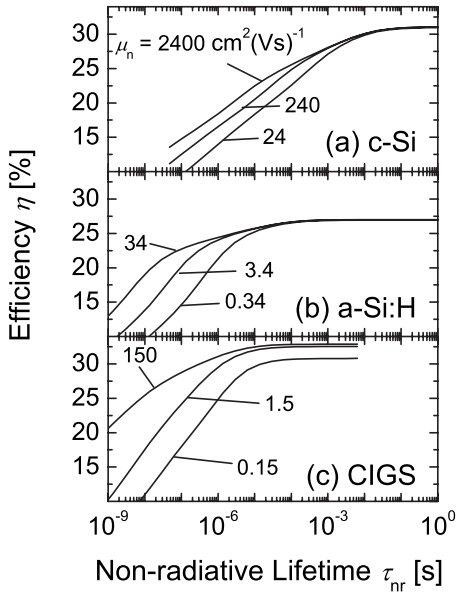

FIG. 10. Simulated efficiency of (a) crystalline silicon (c-Si), (b) hydrogenated amorphous silicon (a-Si:H), and (c) $Cu(In_{1-x}Ga_x)Se_2$ (CIGS, with $x=0.26$) versus nonradiative lifetime. For typical measured values of the electron mobility μ_n, neither c-Si nor a-Si:H is limited by carrier transport in the radiative recombination limit. Only in CIGS, transport might restrict the maximum attainable efficiency in the radiative recombination limit if the mobility is much lower than $\mu_n=1$ cm^2 (V s)$^{-1}$.

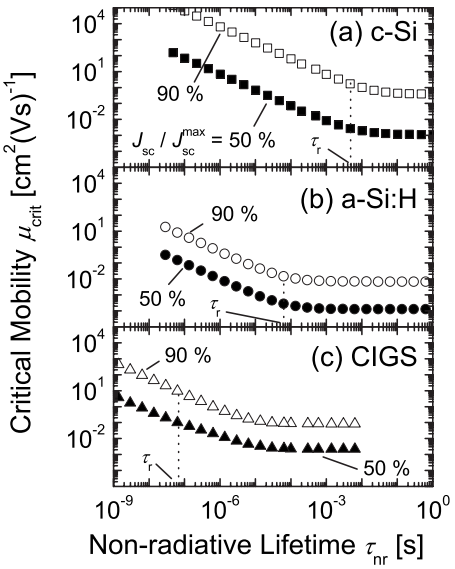

FIG. 11. Critical mobility for crystalline silicon (c-Si), hydrogenated amorphous silicon (a-Si:H), and $Cu(In_{1-x},Ga_x)Se_2$ (CIGS, with $x=0.26$) versus nonradiative lifetime. The critical mobility is inversely proportional to the nonradiative lifetime and saturates once the nonradiative lifetime is much larger than the radiative lifetime τ_r of the respective material. At a doping level $N_A=5\times10^{16}$ cm^{-3}, it holds $\tau_r=4.7\times10^{-3}$ s for c-Si, $\tau_r=6.2\times10^{-5}$ s for a-Si:H, and $\tau_r=6.4\times10^{-8}$ s for CIGS. The saturation level depends linearly on the doping concentration.

$=3.8\times10^{-1}$cm^2 (V s)$^{-1}$. Thus, the mobilities of c-Si are more than 3 orders of magnitude larger than this critical value that would indicate a pure mobility problem for a photovoltaic material, instead of a $\mu\tau$ problem. Such a $\mu\tau$ problem for carrier collection arises if τ_{nr} falls below 10 μs [cf. Fig. 11(a)] like it can be the case in polycrystalline cells.

B. Amorphous silicon

Existing amorphous silicon solar cells suffer from relatively low short circuit currents of $J_{sc}\leqslant17.5$ mA cm^{-2},[36] compared to a limit of $J_{sc}^{SQ}=20.8$ mA cm^{-2} corresponding to a band gap $E_g=1.75$ eV, even though *pin* structures are used to enhance carrier collection. Electron mobilities in intrinsic a-Si:H are in the range $\mu_n=1-5$ cm^2 (V s)$^{-1}$ (see, for example, Refs. 37 and 38). With the critical mobility $\mu_{crit}^{rad}(90\%)=8.5\times10^{-3}$ cm^2 (V s)$^{-1}$, which allows us to collect 90% of the current, these mobilities would be high enough to guarantee complete carrier collection in the radiative recombination limit if the device were only limited by electron transport.

However, electron mobilities are reduced drastically if a-Si:H is doped.[39] This is one reason why a-Si:H solar cells use an intrinsic layer as the photovoltaic absorber within a *pin* structure. Thus, the radiative limit of this type of solar cells is basically out of the scope of the present paper. Nevertheless, we may get a first idea about whether or not the material has an inherent mobility problem. Hereto, we have to look at the lower one of the two carrier mobilities, in this case the hole mobility.

For hole mobilities we have to distinguish between the band mobility μ_p^{band} that accounts for a mobile hole above the mobility edge and the effective drift mobility μ_p^{eff} that takes into account trapping of the carriers in the valence band tails during their transport to the electrical terminal.[40] The band mobility is $\mu_p^{band}=0.3$ cm^2 (V s)$^{-1}$,[40] or even much larger.[41] However, this quantity is irrelevant for the practical working conditions of the device. Values for the relevant drift mobility μ_p^{eff} range between few times 10^{-4} cm^2 (V s)$^{-1}$ and few times 10^{-2} cm^2 (V s)$^{-1}$.[40,41]

When considering a *pin* model that is based on nonradiative recombination Schiff found a critical mobility of about 1 cm^2 (V s)$^{-1}$ which by far exceeds the measured values for μ_p^{eff},[32,40] and therefore proposed the term low-mobility solar cells.[32] As the current considerations show, only the best of the measured values are above the critical value $\mu_{crit}^{rad}(90\%)=8.5\times10^{-3}$ cm^2 (V s)$^{-1}$ that allows us to collect 90% of the available short circuit current density [cf. Fig. 11(b)]. Therefore, the term low-mobility solar cell is most likely even applicable in the radiative limit, i.e., a-Si:H is a photovoltaic material which comes close to having an inherent mobility problem. A detailed analysis of *pin* structures that investigates the interplay between the mobilities of both types of carriers will be given in Ref. 34.

The lesson learned from the example of a-Si:H is that structural disorder (or inhomogeneities) not only reduce the available open circuit voltage of a given photovoltaic absorber material[42–44] but also, and more importantly, the short circuit current even if no loss mechanism other than radiative recombination is present.

C. Cu(In,Ga)Se_2

Solar cell absorbers made from CIGS exhibit mobilities in the range $1-20\ \mathrm{cm}^2\ (\mathrm{V\ s})^{-1}$.[43,45] The critical mobility to achieve 90% of the maximal short circuit current in the radiative recombination limit of Fig. 11(c) is $\mu_{\mathrm{crit}}^{\mathrm{rad}}(90\%)=8\times10^{-2}\ \mathrm{cm}^2\ (\mathrm{V\ s})^{-1}$. Thus CIGS is only one or, at best, 2 orders of magnitude away from having an inherent mobility problem. This implies that as soon as nonradiative recombination comes into play the available short circuit current of a CIGS solar cell falls below the maximum value. Measured diffusion lengths in CIGS are in the range $0.5-1.5\ \mu\mathrm{m}$,[46] approximately corresponding to the thickness of a typical device. Reported lifetimes are in the low nanosecond regime.[47,48] This is about 1 order of magnitude away from the radiative lifetime $\tau_r=64$ ns that we have computed from the absorption data in Fig. 9 and used for the present calculations. From Fig. 11(c), we find that $\tau_{nr}=30$ ns already requires a carrier mobility $\mu_{\mathrm{crit}}(90\%)\approx20\ \mathrm{cm}^2\ (\mathrm{V\ s})^{-1}$ to warrant a 90% carrier collection. High efficiency CIGS cells actually suffer a loss of slightly less than 10% in their short circuit current due to recombination in the absorber material (see, e.g., Ref. 49). However, carrier collection in these devices is enhanced by the electrical field in the space charge region and by band gap grading.[50,51]

V. CONCLUSION

This paper has investigated the effect of finite carrier mobility on the performance of solar cells and LEDs close to their radiative limit. We find that four quantities, namely, the absorption coefficient, the doping density, the device thickness, and the light trapping scheme, immediately gain fundamental importance once finite mobilities are considered. Our model generalizes the SQ theory of ideal *pn*-junction solar cells (and ideal LEDs) to situations where restrictions by diffusive carrier transport become decisive. We find that solar cells are more sensitive to low carrier mobilities than LEDs. In turn, nonradiative recombination harms more the performance of LEDs than that of solar cells. For the case of an energy-independent absorption coefficient α, we find a simple expression for the critical mobility $\mu_{\mathrm{crit}}^{\mathrm{rad}}$ that is necessary to extract 50% of the available short circuit current density in the radiative limit.

Such an analytical approach is not possible for real semiconductor materials where the functional dependence of α on the photon energy is not given by a simple step function. Here, experimental values of α have to be used to simulate the dependence of the conversion efficiency on the carrier mobility. By this method we find critical mobilities $\mu_{\mathrm{crit}}^{\mathrm{rad}}(90\%)$ that allow collection of 90% of the available short circuit current.[22] We find mobilities $\mu_{\mathrm{crit}}^{\mathrm{rad}}(90\%)=0.38$, 0.007, and $0.08\ \mathrm{cm}^2\ (\mathrm{V\ s})^{-1}$ for the materials crystalline silicon, amorphous silicon, and CIGS.

Typical mobilities of crystalline silicon are about 3 orders of magnitude larger than the critical value, thus, ruling out any inherent mobility problem for this material. In CIGS, this difference is only about 1 order of magnitude whereas in *a*-Si:H the experimental drift mobilities for holes are scattered around the critical value. Therefore in its radiative limit and all the more in practice,[32,40] *a*-Si:H must be considered as an inherent low-mobility material. Even the help of the built-in field in a *pin* structure only partly compensates this problem.[32,40,52] In practical CIGS solar cells, the relatively low mobilities combined with the presence of nonradiative recombination implies some losses in the short circuit current density. Therefore, high efficiency CIGS devices[53,54] use a three-stage process[55] leading to a band gap grading that enhances carrier collection by the resulting quasielectrical field.[50,51]

It is interesting to note that such collection enhancement by means of built-in (quasi-) electric fields is not possible in excitonic solar cells made from organic semiconductors. This type of device relies on the diffusive transport of coupled (and therefore neutral) electron and/or hole pairs (excitons).[56,57] The relatively low mobility of excitons in such materials (for reviews, see Refs. 58–60) might be a limiting factor for the short circuit current despite of their very high absorption coefficients and their favorable ratio between radiative and nonradiative lifetimes. Due to the relative insensitivity of LEDs on low mobilities as discussed in Sec. III E, such organic semiconductors are well suited for light-emitting diodes[61] while for solar cell applications additional efforts such as blending of the polymers with C_60 atoms[62] is necessary to overcome the mobility problem. An investigation of mobility effects in excitonic as well as electronic solar cells that use the mathematical tools outlined in the present paper and also include space-charge effects will be published elsewhere.[34]

ACKNOWLEDGMENTS

The authors are grateful for support by the German Ministry for Education and Research (BMBF) (Contract No. 03SF0308E). The authors also thank G. Gläser and T. Kirchartz for valuable discussions.

APPENDIX: DERIVATION OF RADIATIVE INTERACTION FUNCTION

The radiative interaction term f_r^{Lamb} consists of all optical propagation paths that at least once include the Lambertian front surface of the cell. Therefore, we consider the total balance between the photon flux ϕ_{em} emitted from the surface into the cell and the photon flux ϕ_{rec} that is received by the surface from the cell's interior (cf. Fig. 12). The probability that a photon from the interior of the cell is reflected back into the cell's interior is $1-t_{\mathrm{Lamb}}$, where the average transmission probability t_{Lamb} of a Lambertian surface with zero reflectance is $t_{\mathrm{Lamb}}=1/\bar{n}^2$. Balancing the photon fluxes at the front surface therefore yields $\phi_{\mathrm{em}}=(1-t_{\mathrm{Lamb}})\phi_{\mathrm{rec}}$. Additionally, any photon emitted from the surface traverses the cell and reaches the front surface again with a probability t_{cell}. Therefore, it also holds $\phi_{\mathrm{rec}}=t_{\mathrm{cell}}\phi_{\mathrm{em}}+\phi_r$, including the photon flux ϕ_r that is generated by radiative recombination in x_r. Resolving for ϕ_{em} yields

$$\phi_{\mathrm{em}}=\phi_r\frac{1-t_{\mathrm{Lamb}}}{1-t_{\mathrm{cell}}(1-t_{\mathrm{Lamb}})}. \tag{A1}$$

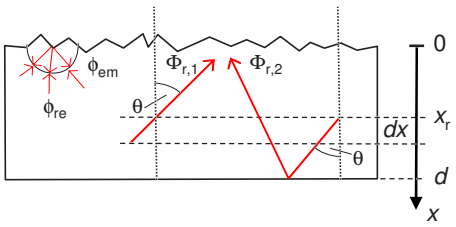

FIG. 12. (Color online) Solar cell with textured surface. The photon flux emitted from the front surface into the cell's interior is denoted as ϕ_{em}. The flux ϕ_{rec} received by the front surface from emission from radiative recombination in x_r includes the direct flux $\phi_{r,1}$ and the flux $\phi_{r,2}$ reflected once at the back side.

The transmission probability t_{cell} is obtained by integration over a normalized Lambertian angular distribution[23]

$$t_{cell} = \int_0^{\pi/2} 2 \exp\left[\frac{-2\alpha d}{\cos(\theta)}\right]\cos(\theta)\sin(\theta)d\theta = (1-2\alpha d)\exp(-2\alpha d) + (2\alpha d)^2\,\mathrm{Ei}(2\alpha d). \quad \text{(A2)}$$

Next, we calculate

$$\delta\phi_{r,1/2}(x_g,x_r) = \frac{4\pi\bar{n}^2}{h^3c^2}\int_0^{\infty}\alpha(E)E^2\exp\left(\frac{-E}{k_BT}\right) \times \int_0^{\pi/2}\exp\left[\frac{-\alpha\delta_{1/2}}{\cos(\theta)}\right]\sin(\theta)d\theta dE\frac{n(x_r)}{n_0}\delta x_r, \quad \text{(A3)}$$

where $\delta_1 = x_r$ and $\delta_2 = 2d - x_r$. The corresponding radiative interaction function is

$$f_{r,1/2}(0,x_r) = \int_0^{\pi/2}\exp\left[\frac{-\alpha\delta_{1/2}}{\cos(\theta)}\right]\sin(\theta)d\theta = \mathrm{Ei}_2(\alpha\delta_{1/2}). \quad \text{(A4)}$$

Accordingly, the interaction function describing the interaction between the Lambertian front surface and the plane in x_g reads as

$$f_{r,1/2}(x_g,0) = \int_0^{\pi/2}\exp\left[\frac{-\alpha\delta_{1/2}}{\cos(\theta)}\right]\sin(\theta)d\theta = \mathrm{Ei}_2(\alpha\delta_{1/2}), \quad \text{(A5)}$$

where $\delta_1 = x_g$ and $\delta_2 = 2d - x_g$. Therefore, the overall radiative interaction function between x_r and x_g via multiple reflections at the Lambertian front surface is given by

$$f_r^{Lamb}(x_g,x_r) = 2\{f_{r,1}(0,x_r) + f_{r,2}(0,x_r)\}\frac{1-t_{Lamb}}{1-t_{cell}(1-t_{Lamb})}\{f_{r,1}(x_g,0) + f_{r,2}(x_g,0)\} = \frac{2(1-t_{Lamb})\{\mathrm{Ei}_2(\alpha x_r) + \mathrm{Ei}_2(2\alpha d - \alpha x_r)\}\{\mathrm{Ei}_2(\alpha x_g) + \mathrm{Ei}_2(2\alpha d - \alpha x_g)\}}{1-t_{cell}(1-t_{Lamb})}. \quad \text{(A6)}$$

*Present address: Q-Cells AG, 06766 Thalheim, Germany; j.mattheis@q-cells.com

[1] W. Shockley and H. J. Queisser, J. Appl. Phys. **32**, 510 (1961).
[2] M. A. Green, *Solar Cells: Operating Principles, Technology, and System Applications* (Prentice-Hall, Englewood Cliffs, 1982).
[3] W. Shockley, Bell Syst. Tech. J. **28**, 435 (1949).
[4] A. Martí, J. L. Balenzategui, and R. F. Reyna, J. Appl. Phys. **82**, 4067 (1997).
[5] W. P. Dumke, Phys. Rev. **105**, 139 (1957).
[6] T. S. Moss, Proc. Phys. Soc. London, Sect. B **70**, 247 (1957).
[7] P. T. Landsberg, Proc. Phys. Soc. London, Sect. B **70**, 1175 (1957).
[8] W. N. Carr, Infrared Phys. **6**, 1 (1966).
[9] S. Kameda and W. N. Carr, J. Appl. Phys. **44**, 2910 (1973).
[10] C. J. Hwang, Phys. Rev. B **6**, 1355 (1972).
[11] F. Stern and J. M. Woodall, J. Appl. Phys. **45**, 3904 (1974).
[12] T. Kuriyama, T. Kamiya, and H. Yanai, Jpn. J. Appl. Phys. **16**, 465 (1977).
[13] P. Asbeck, J. Appl. Phys. **48**, 820 (1977).
[14] K. Mettler, Phys. Status Solidi A **49**, 163 (1978).
[15] J. E. Parrott and A. Potts, in Conference record of the 22nd IEEE Photovoltaics Specialist Conference, 1991 (Conference record), p. 153.
[16] S. M. Durbin and J. L. Gray, in Conference record of the 22nd IEEE Photovoltaics Specialist Conference, 1991 (Conference record), p. 188.
[17] S. M. Durbin and J. L. Gray, IEEE Trans. Electron Devices **41**, 239 (1994).
[18] V. Badescu and P. Landsberg, Semicond. Sci. Technol. **12**, 1491 (1997).
[19] A. Yamamoto, M. Kurizuka, M. M. Murshid, M. Ohkubo, and A. Hashimoto, Sol. Energy Mater. Sol. Cells **50**, 259 (1998).
[20] J. L. Balenzategui and A. Martí, Sol. Energy Mater. Sol. Cells **90**, 1068 (2006).
[21] J. E. Parrott, Sol. Energy Mater. Sol. Cells **30**, 221 (1993).
[22] J. Mattheis, Ph.D. thesis, University of Stuttgart, 2008.
[23] M. A. Green, Prog. Photovoltaics **10**, 235 (2002).
[24] R. Hulstrom, R. Bird, and C. Riordan, Sol. Cells **15**, 365 (1985).
[25] T. Tiedje, E. Yablonovitch, G. Cody, and B. Brooks, IEEE Trans. Electron Devices **ED-31**, 711 (1984).

[26] E. Yablonovitch, J. Opt. Soc. Am. **72**, 899 (1982).
[27] U. Rau, Phys. Rev. B **76**, 085303 (2007).
[28] T. Kirchartz, U. Rau, M. Kurth, J. Mattheis, and J. H. Werner, Thin Solid Films **515**, 6238 (2007).
[29] W. v. Roosbroeck and W. Shockley, Phys. Rev. **94**, 1558 (1954).
[30] S. Sze, *Semiconductor Devices: Physics and Technology* (Wiley, New York, 2002).
[31] L. Ley, in *The Physics of Hydrogenated Amorphous Silicon II*, edited by J. D. Joannopopoulos and G. Lucovsky (Springer, Heidelberg, 1984).
[32] E. A. Schiff, Sol. Energy Mater. Sol. Cells **78**, 567 (2003).
[33] K. Orgassa, Ph.D thesis, University of Stuttgart, 2004.
[34] T. Kirchartz and U. Rau (unpublished).
[35] P. J. Rostan, U. Rau, V. X. Nguyen, T. Kirchartz, M. B. Schubert, and J. H. Werner, Sol. Energy Mater. Sol. Cells **90**, 1345 (2006).
[36] J. Meier, J. Sitznagel, U. Kroll, C. Bucher, S. Fay, T. Moriarty, and A. Shah, Thin Solid Films **451**, 518 (2004).
[37] E. A. Schiff, R. I. Devlen, H. T. Grahn, and J. Tauc, Appl. Phys. Lett. **54**, 1911 (1989).
[38] G. Juška, K. Arlauskas, J. Kočka, M. Hoheisel, and P. Chabloz, Phys. Rev. Lett. **75**, 2984 (1995).
[39] J. A. Howard and R. A. Street, Phys. Rev. B **44**, 7935 (1991).
[40] E. A. Schiff, J. Non-Cryst. Solids **352**, 1087 (2006).
[41] Q. Gu, Q. Wang, E. A. Schiff, Y.-M. Li, and C. T. Malone, J. Appl. Phys. **76**, 2310 (1994).
[42] U. Rau and J. H. Werner, Appl. Phys. Lett. **84**, 3735 (2004).
[43] J. H. Werner, J. Mattheis, and U. Rau, Thin Solid Films **480**, 399 (2005).
[44] J. Mattheis, U. Rau, and J. H. Werner, J. Appl. Phys. **101**, 113519 (2007).
[45] J. Lee, J. D. Cohen, and W. N. Shafarman, Thin Solid Films **480**, 336 (2005).
[46] U. Rau and H.-W. Schock, Appl. Phys. A: Mater. Sci. Process. **69**, 131 (1999).
[47] K. Puech, S. Zott, K. Leo, M. Ruckh, and H.-W. Schock, Appl. Phys. Lett. **69**, 3375 (1996).
[48] B. Ohnesorge, R. Weigand, G. Bacher, and A. Forchel, Appl. Phys. Lett. **73**, 1224 (1998).
[49] U. Rau, in *Advances in Solid State Physics 44*, edited by B. Kramer (Springer, Heidelberg, Germany, 2004), p. 27.
[50] J. Mattheis, P. J. Rostan, K. Orgassa, U. Rau, and J. H. Werner, Sol. Energy Mater. Sol. Cells **91**, 689 (2007).
[51] M. Topič, F. Smole, and J. Furlan, J. Appl. Phys. **79**, 8537 (1996).
[52] R. S. Crandall, J. Appl. Phys. **55**, 4418 (1984).
[53] K. Ramanathan, M. A. Contreras, C. L. Perkins, S. Asher, F. S. Hasoon, J. Keane, D. Young, M. Romero, W. Metzger, R. Noufi, J. Ward, and J. Duda, Prog. Photovoltaics **11**, 225 (2003).
[54] P. Jackson, R. Würz, U. Rau, J. Mattheis, M. Kurth, T. Schlötzer, G. Bilger, and J. H. Werner, Prog. Photovoltaics **15**, 507 (2007).
[55] A. Gabor, J. Tuttle, D. S. Albin, M. Contreras, R. Noufi, and A. Hermann, Appl. Phys. Lett. **65**, 198 (1994).
[56] B. A. Gregg, J. Phys. Chem. B **107**, 4688 (2003).
[57] B. A. Gregg and M. C. Hanna, J. Appl. Phys. **93**, 3605 (2003).
[58] H. Hoppe and N. S. Sariciftci, J. Mater. Res. **19**, 1924 (2004).
[59] S. E. Gledhill, B. Scott, and B. A. Gregg, J. Mater. Res. **20**, 3167 (2005).
[60] M. Graetzel, MRS Bull. **30**, 23 (2005).
[61] N. K. Patel, S. Cinà, and J. H. Burroughes, IEEE J. Sel. Top. Quantum Electron. **8**, 346 (2002).
[62] N. S. Saricifci, L. Smilowitz, A. J. Heeger, and F. Wudl, Science **258**, 1474 (1992).